NAL PROPOSAL No. 54

Correspondent: J. Pine
Calif. Inst. of Tech.
Pasadena, Ca. 91109

FTS/Off-net: 213-688-2000
795-6841

QUASI-TWO-BODY REACTIONS AT 50-200 GeV

A. Dzierba, R. Gomez, Y. Nagashima, J. Pine
Caltech

P. Schlein, W. Slater
UCLA

E. Malamud
NAL

June 6, 1970

June 6, 1970

QUASI-TWO-BODY REACTIONS AT 50-200 GeV

Abstract

We propose a wire spark chamber experiment to study peripheral reactions which lead to a final state containing one or more resonances. An example is $\pi^+ p \rightarrow \rho^0 \Delta^{++}$. The experiment is intended to measure a variety of such processes simultaneously, for pions, kaons, and protons incident on protons. The range of four-momentum transfers will be from essentially zero to about 1 $(GeV/c)^2$. The major goals of the experiment may be summarized as follows:

1. To study the s and t dependence of the cross sections for peripheral processes in order to check various dynamical models.
2. To search for new meson and baryon resonances and in favorable cases to determine their quantum numbers.
3. To study π-π and K-π scattering in those reactions which produce baryon resonances predominantly by pion exchange.

Experimenters

A. Dzierba, R. Gomez, Y. Nagashima, J. Pine - Caltech

P. Schlein, W. Slater - UCLA

E. Malamud - NAL

Correspondent

J. Pine - Caltech

Table of Contents

I. Physics Justification

At the energies currently available for high energy physics, a wide variety of quasi-two-body reactions have been studied. Schematically, such reactions may be represented by the graph below.

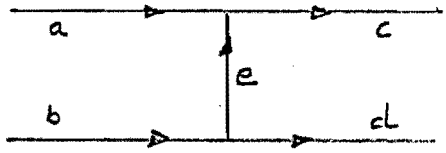

Incident particles a and b are transformed into c and d after exchange of a particle e. Only in a limited number of reactions are c and d stable particles. Otherwise, they may be any of a variety of meson and baryon resonances.

The diagram above is expected to describe highly peripheral processes, characterized by low values of four momentum transfer. Currently, the different dynamical theories of peripheral interactions include particle exchange, Regge poles, Regge cuts, and the droplet and eikonal models. The peripheral interactions have been a very important area for interplay between theory and experiment. Extending information about such reactions to higher energies at NAL is almost certain to have a strong impact on our thinking.

There are a few general comments which can be made about the study of quasi-two-body reactions at NAL energies in comparison with studies being made at present energies.

1. There will be better separation in the laboratory between the decay products of the forward and backward (cm. system) resonances. For example, at 100 GeV for $\pi^+ p \rightarrow \rho\Delta^{++}$, the π^+ from the ρ^o is within two degrees of the beam direction, with momentum greater than 2.5 GeV/c, for all ρ decays. The π^+ from the Δ^{++} is never in

this kinematic region.

2. For production of two final state resonances with given masses, the minimum four-momentum transfer at 100 GeV is a factor of 10 less than at 10 GeV. The very low t region will be accessible at NAL, even for relatively large masses.

3. As a consequence of the two preceding comments, the chance for discovery of presently unknown higher mass resonances is enhanced at NAL.

4. A majority of quasi-two-body reactions (those which do not occur diffractively) have cross sections which rapidly decrease with energy. It is therefore unlikely that the bubble chamber will maintain the dominant role it has so far enjoyed for the study of these processes.

We are proposing an experiment which utilizes counters and spark chambers to detect some of the multiparticle final states characteristic of quasi-two-body reactions. The expected counting rate for a microbarn cross section is about 1000/day. The experiment is designed for the energy range from 50-150 GeV. The variety of reactions accessible with this experiment is too broad for a full discussion of all of them. In what follows we will try to discuss some concrete examples of processes which are typical, and which we feel might be among the more significant aspects of the experiment. The apparatus is not by any means a completely general detector, and the examples will illustrate two conditions established by the experimental setup: (1) That there be no neutrons involved, and (2) that there be no gamma rays or neutral pions outside of a small forward cone. Even with these conditions, the number of interesting reactions is very large.

A. Meson Exchanges

Consider the reaction

$$\pi^+ p \rightarrow \rho^o \Delta^{++} .$$

At present energies the one pion exchange model seems successful here, and it is interesting from the standpoint of Regge theory that this is true in spite of the fact that the A_2 trajectory lies above the pion trajectory. It could be that at NAL energies the A_2 exchange will become important. The ρ^o and Δ^{++} density matrix elements will be determined to check the OPE assumption, and the cross section as a function of s and t will be compared with various theories.

Another reaction which will be important to study in order to compare the results with Regge theories is

$$\pi^+ p \rightarrow \pi^o \Delta^{++}$$

This reaction is thought to proceed by ρ exchange and exhibits the same t dependence, with a dip at t = -0.6, as the $\pi^- p$ charge exchange scattering. It will be important to observe whether the dip exhibits an s dependence in either its strength or its t value. Other interesting final states for the $\pi^+ p$ reaction are $f^o \Delta^{++}$(ρ, A_2 exchange), $\omega^o \Delta^{++}$ (ρ exchange) and $\eta^o \Delta^{++}$ (A_2 exchange).

Two reactions which we hope to measure, and which are thought to proceed via K*(890) and K*(1420) exchange are

$$\pi^- p \rightarrow K^o \Lambda^o$$

$$K^- p \rightarrow \pi^o \Lambda^o .$$

Comparison of these two cross sections is a means of testing exchange degeneracy for the two K* trajectories. The evidence at lower energies is not very conclusive, and data at high energies for this reaction and others involving exchange degeneracy will be interesting.

B. New Resonances

The experiment proposed here is appropriate for detecting new resonances. The efficiency is high for meson resonances with masses up to at least 4 GeV and for baryon resonances up to somewhat lower masses. The details of the mass resolutions and solid angle acceptances are presented in the summary which begins the section titled Experimental Arrangement. While the apparatus is not the last word in high resolution missing mass devices it has good characteristics for a general survey.

C. Non-Resonant Meson Interactions

At lower energies it has been possible to study π-π and K-π scattering by Chew-Low extrapolation for reactions dominated by one pion exchange. Schlein has discussed the promising results for Δ^{++} final states (NAL 1969 Summer Study, Vol 2, p. 8), and three relevant Δ^{++} reactions are

$$pp \rightarrow (\pi^- p)\ \Delta^{++}$$

$$\pi^+ p \rightarrow (\pi^+ \pi^-)\ \Delta^{++}$$

$$K^+ p \rightarrow (K^+ K^-)\ \Delta^{++}\ .$$

The first reaction is important as a check, since the result ($\pi^- p$ scattering) is known. The others measure π-π and K-π elastic scattering. In addition, there will be an opportunity to analyze data in which the final meson state is not specified to try to extract total cross sections.

D. Diffraction Dissociation (Pomeron Exchange)

The experiment is aimed at studying processes with cross sections of one microbarn or less, and therefore a trigger which accepts diffractive processes is likely to swamp the spark chamber system. We anticipate that by running the apparatus for one day with a trigger that accepts reactions which can go by Pomeron exchange we will accumulate about 10^5 such events. It is certainly worthwhile to collect such data in an early experiment although much of the detailed physics may ultimately be done better in a triggered bubble chamber experiment.

A typical process which will be of interest is

$$\pi^+ p \rightarrow (\pi^+\pi^-\pi^+)N^{*+}.$$

While this reaction need not proceed solely by Pomeron exchange, if present theoretical ideas are correct, meson exchange will be negligible at 100 GeV compared to Pomeron exchange. (The presence or absence of the Δ resonances will be a sensitive check for I = 1 meson exchanges, since they cannot be produced diffractively.) The study of this reaction as a function of s, t, and the mass of the three pion system will be important in checking expectations based on diffractive dissociation of the pion. The presence or absence of known resonances can be used to check theoretical predictions of spin, parity, and helicity rules for diffractive processes. The data will also be useful in looking for new meson and baryon resonances with the quantum numbers of the pion and nucleon.

E. Baryon Exchange

In contrast to the Pomeron exchange processes, we anticipate that these cross sections may be so small that too little data will be obtained for detailed interpretation. A sample pair of reactions which we will look for is

$$\pi^+ p \to \Delta^{++} \text{ (forward)} + \rho^0$$

$$\pi^- p \to N^{*0} \text{ (forward)} + \rho^0$$

In view of our relatively poor knowledge of baryon exchanges, any data on the s and t dependence of these reactions will be useful. Furthermore, study of the density matrix of a backward-going meson resonance provides rigid constraints on the Regge parameters of the exchanged baryon.

II. Experimental Arrangement

A. Summary

In this section we will describe how the experiment is to be done. Succeeding sections contain more information about some of the experimental details, to back up the statements made here and to provide the interested reader with enough material to check our conclusions.

The sketch below shows a plan view of the major items of the experimental apparatus.

1. Beam
2. Target
3. Target spectrometer (also see Section II-B)
4. Forward spectrometer (also see Section II-C)
5. Gas Cerenkov counter (also see Section II-D)
6. Gamma ray detector

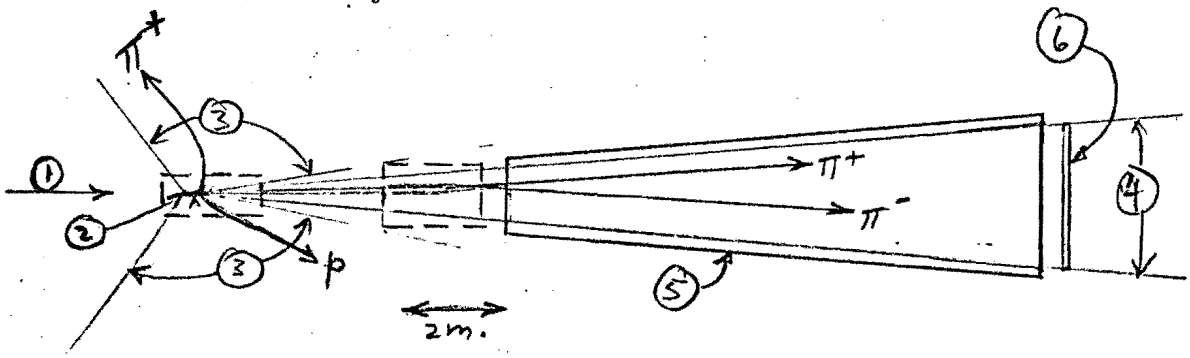

Two wire-chamber magnet spectrometers are indicated schematically by dotted lines which outline the magnet poles and solid lines which indicate the solid angle they cover. Four charged particle trajectories, representing a "typical" $\rho^{o}\Delta^{++}$ final state are also shown.

The philosophy of the experiment is that the states which are studied are only those for which all the decay products are charged. (Exceptions are made for the case of a forward π^{o}, which will be discussed separately.)

Furthermore, it is assumed that the identities of the particles are known: p, π, K, etc. In this case, moderately accurate momentum measurements suffice to determine the mass of each of two resonances with good accuracy. If the spectrometers were used to determine the energy and momentum balance well enough to detect the presence of a slow missing π^{o}, then much more accurate momentum measurements, and consequently larger spectrometers, would be needed.

The desired reaction topology for triggering the spark chambers is determined by counters which surround the target. There are lead-scintillator shower counters for detecting gamma rays over the entire solid angle except for a narrow forward cone.* These are in veto in the trigger. There are scintillation counters for detecting charged particles outside the region subtended by the spectrometers, also in veto.

In the useful solid angle of the experiment there are scintillation counter hodoscopes which determine the number of forward charged particles and the number of charged particles in the solid angle subtended by the target spectrometer. The trigger essentially consists of requirements on the outputs of these hodoscopes in conjunction with the vetoes previously mentioned. For normal running, we will usually select events with two charged particles in each spectrometer region. This very strongly biases us against diffractive processes. In order to measure diffractive processes, the trigger will accept three forward-going charged particles and one or three charged particles in the target spectrometer.

At present energies the decay products of particle systems moving forward and backward in the c.m. system are not well separated in the lab. However, at NAL energies the separation should be excellent, facilitating

*These counters veto gamma rays and not charged particles. They have a front scintillator viewed by one phototube followed by a shower counter viewed by another phototube.

the use of the simple triggers outlined above. When the trigger requirements are fulfilled, the wire spark chambers associated with the spectrometers are triggered and particle trajectories are determined. The spectrometer performance is summarized below.

Spectrometer	Acceptance (Square Degrees)	Momentum Range (GeV/c)	Momentum Accuracy (%)	Two Body Mass Accuracy (%)
Target	(135x90) to right and left	0.2-3.0	~5%	(1-3%), 1 to 3 GeV
Forward	2.5x5	3.0-100	(1-2)%	1%, 1 to 4 GeV

The table gives rough averages over a wide range of momentum and angles, but more detailed spectrometer information appears in the following sections. Some specific examples of expected mass resolutions are as follows:

Target spectrometer: $M(\pi p) = 1238$; $\Delta M = \pm 10$ MeV

$M(\pi p) = 2000$; $\Delta M = \pm 40$ MeV

Forward spectrometer: $M(\pi\pi) = 750$; $\Delta M = \pm 10$ MeV

$M(\pi\pi) = 2000$; $\Delta M = \pm 18$ MeV

$M(\pi\pi) = 4000$; $\Delta M = \pm 28$ MeV

The particle identification is made in various ways, but the most important aid is the gas Cerenkov counter. For normal running this

counter will usually be operated for optimum differentiation of π's and K's, in which case it permits positive separation of two-meson resonances into π-π. π-K, and K-K with an efficiency between about 50 and 100%, depending on the resonance mass. The gas Cerenkov counter can also be run for good differentiation of protons from mesons, but not simultaneously with good π-K separation.

At the target spectrometer there are three items of data which aid in distinguishing protons from mesons:

a) The charge, for states with negative mesons.

b) The two-body kinematics, except at the symmetrical angle.

c) The energy loss in the hodoscope counters.

For distinguishing kaons from pions, the first method above is not available and the other two do not work as well as for proton-meson identications. However, the presence of K meson at the target spectrometer can be inferred from the presence of a forward K via conservation of strangeness. In an analogous way, conservation of baryons will help in overdetermining proton-meson identifications.

This concludes the description of how the experiment operates for reactions producing only charged particles. The gamma ray detector behind the forward spectrometer is used for two additional types of forward going final states:

1. A single neutral meson which decays into two gammas (a π^{o}, an η^{o}, or perhaps a presently unknown meson).

2. Two charged mesons and one neutral one, such as the A_2.

For a great majority of the reactions of type 1 which produce either π^{o} or η^{o} mesons the two gamma rays will strike the detector within an area about 30 cm. square at the center of the detector. This small region can

well have a high-quality combination of wire chambers and counters which locate the gamma ray showers, determine which has the higher energy, and measure the total energy, to a few percent. As a result, we expect to be able to measure the transverse momentum of the neutral meson to within about 30 MeV/c, thereby determining the four-momentum transfer very well. There will be a degree of redundancy which can be used to help check that the reaction is the correct one, and it will be easy to distinguish π^o mesons from η^o mesons.

For reactions of type 2, the neutral meson will sometimes strike the high quality central detector too. However, in order to have good solid angle coverage for high masses a larger gamma ray detector, about 1.5 x 3 meters in area will be constructed. This detector will simply be a layer of lead in front of a wire chamber plane, or perhaps two layers and two wire chamber planes. Good enough positional accuracy of the showers will be obtained so that by momentum balance, using the charged particle data, a reasonable 3π mass measurement can be made. The accuracy will be between about 1.5 and 6%, depending upon the value of the mass and the sharing of momentum among the mesons. For high masses the accuracy is best.

A Sigma 2 computer will process the wire chamber data and counter information, and will simultaneously monitor the overall performance of the apparatus. At a trigger rate of about 10/pulse, the Sigma 2 system will perform on-line preliminary data reduction on all triggers. Both the raw data and the preliminary results will be logged on tape. For the particles in the forward spectrometer the preliminary analysis will be very good, while for particles in the target spectrometer - with its very non-uniform field - the analysis will need later refinement.

The experimenters will thus have on-line information about the physics output of the experiment as well as about the performance of the apparatus. Most of this computer system will be debugged and utilized during the coming year in a hybrid bubble chamber-wire chamber experiment at SLAC. More details of the computer facilities which we plan to use will be found in Section III.

Summing up this section, we believe that we have proposed an apparatus of a size comparable to present day experiments, which requires a minimum of new development work and of new capital investments, which utilizes many resources which we already possess, and which can provide high quality data on a great variety of interesting strong interactions.

B. Target Spectrometer

1. Kinematics

For this experiment, the major emphasis will be on events in which the target spectrometer is used to observe only those baryon or hyperon resonances decaying into two charged particles, a proton and meson:

$$N^* \rightarrow p + \pi^{+}_{-}$$

$$Y^* \rightarrow p + K^{+}_{-}$$

Except for very low mass Y*'s, the kinematics for either case are very similar at a given mass so $N^* \rightarrow p + \pi$ will be the example used in much of the discussion of the target spectrometer.

At minimum four momentum transfer, t_{min}, the N* is produced at zero degrees in the laboratory, with momentum and energy determined by the equation

$$(E - m_p)^2 - (p)^2 = t_{min} \quad .$$

Furthermore, for double resonance production, t_{min} is given by

$$t_{min} \doteq \frac{(M_m^2 - M_o^2)\,(M_b^2 - m_p^2)}{W^2} \quad ,$$

where W is the c.m. energy, M_b is the mass of the baryon resonance, and M_m is the mass of the meson resonance, and M_o is the incident mass.

As an example, consider the reactions $\pi + p$ going to:

a) $\rho_{750} + N^*_{1238}$

b) $\rho_{2000} + N^*_{2000}$,

where the subscripts indicate masses. The 2 GeV case represents a typical higher mass example. We expect for the peripheral processes of interest that the important range of t will extend from t_{min} to roughly 0.5 $(GeV/c)^2$. Figures 1 and 2 show graphically the laboratory momentum and angle distributions for the two examples at these values of t.

For case (a) the laboratory kinematics depend quite strongly on t, while for case (b) than do not. Two general kinematic features for the range of N* masses and momentum transfers of interest are illustrated in the figures:

(1) Particles moving at lab angles greater than about 135 degrees are relatively rare.

(2) For particles near 90 degrees in the lab, momenta are typically < 1 GeV/c, while at more forward angles the momenta may be several GeV/c.

A third kinematic remark can also be added:

(3) For mesons emitted near 180 degrees in the rest frame of the forward going meson resonance, the laboratory momenta are often < 10 GeV/c, and the angles typically range from about 0 to 30 degrees. (See Figure 10.)

Finally, we have checked the kinematics for decay of slow mesons which may originate from baryon exchange processes. Figure 3 shows that a system optimized for the baryon resonances will also handle these decays quite adequately. We will utilize the target spectrometer as an important part of the measuring system for these meson resonance particles.

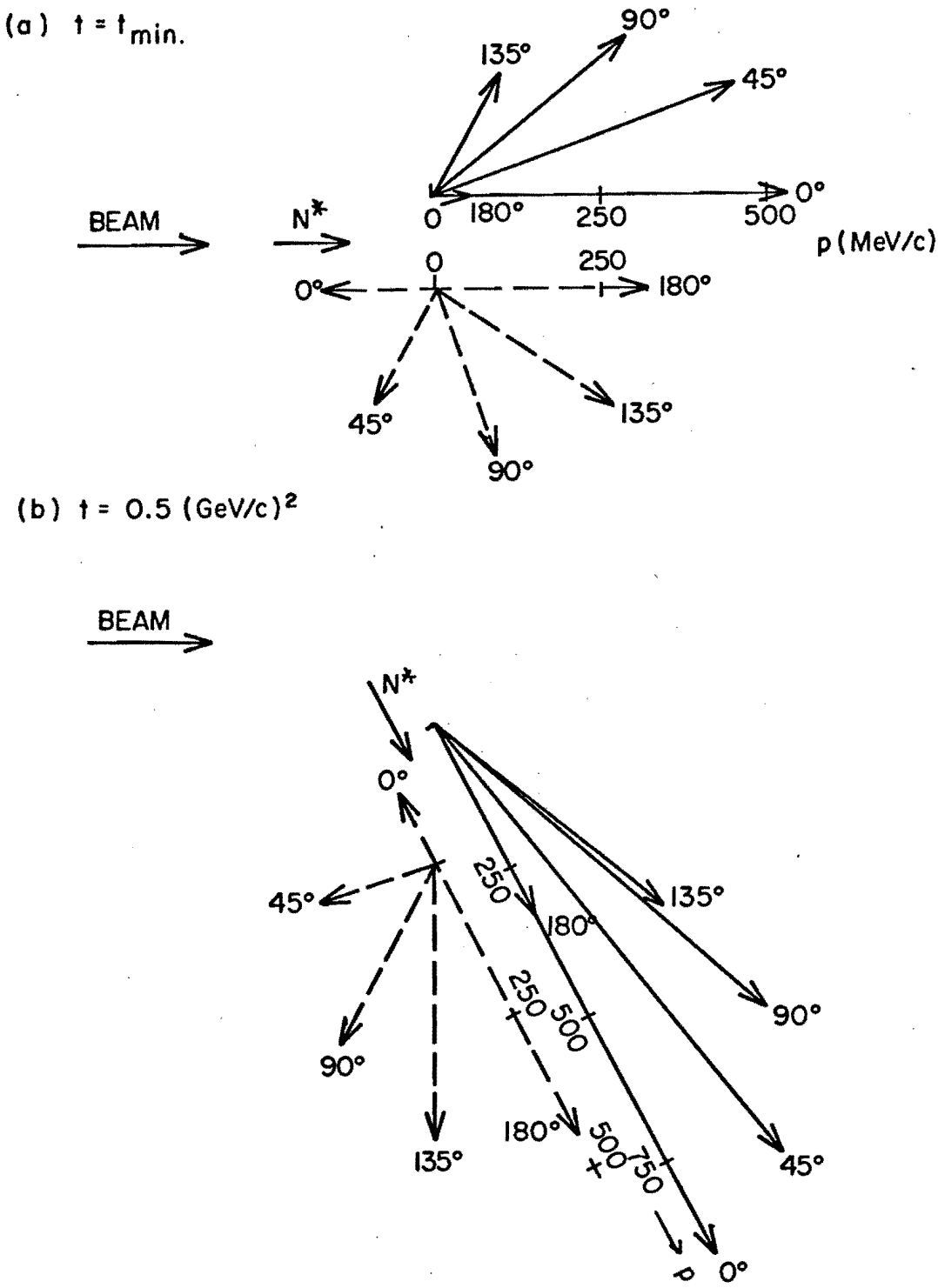

Figure 1. Laboratory kinematics for the decay $\Delta_{1238} \rightarrow \pi p$: (a) for production in πp collisions at minimum t, and (b) for production with $t = 0.5\ (GeV/c)^2$. The solid lines are momentum vectors in the laboratory for the proton, and the dashed lines are for the meson. The angles refer to decay angles in the cm. system of the Δ_{1238}, with zero degrees along its direction of motion.

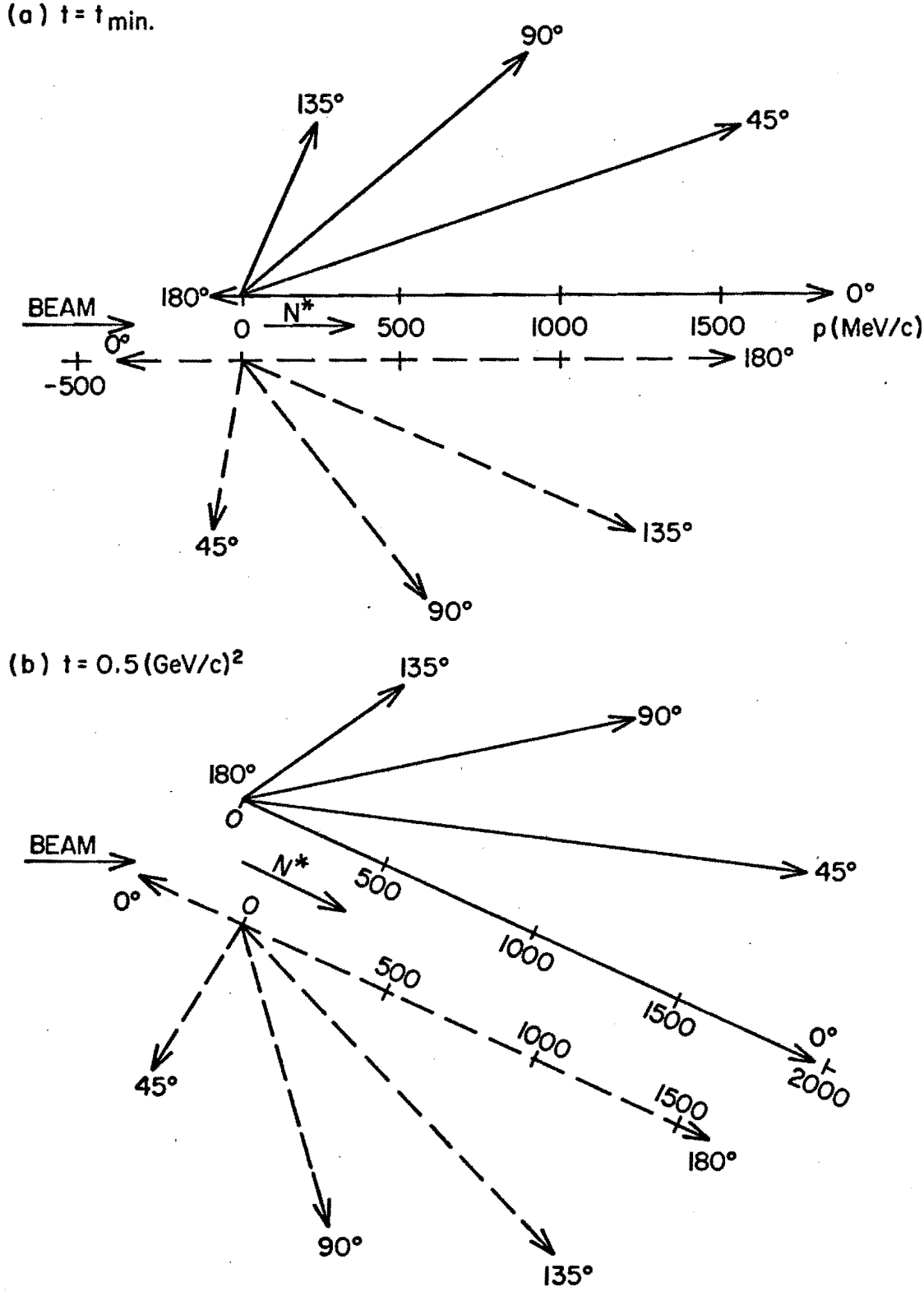

Figure 2. Laboratory kinematics for the decay $N^*_{2000} \rightarrow \pi p$: (a) for production in πp collisions at minimum t, and (b) for production with $t = 0.5(\text{GeV/c})^2$. As in the preceding figures, the solid and dotted lines are proton and pion laboratory momentum vectors.

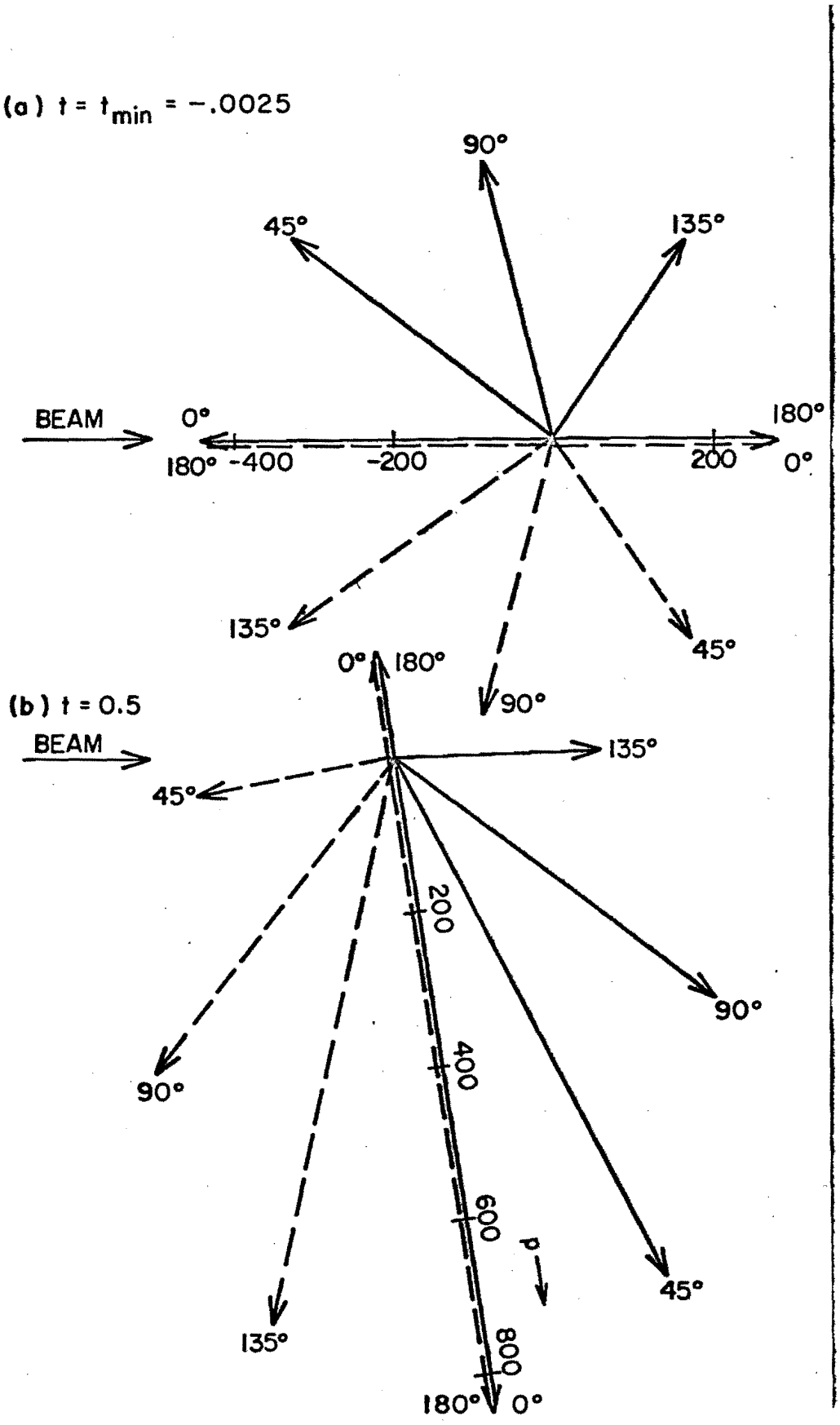

Figure 3. Laboratory kinematics for the decay $\rho \rightarrow 2\pi$: (a) for production by baryon exchange in πp collisions at minimum t, and (b) for production with $t = 0.5(\mathrm{GeV/c})^2$.

2. Magnet

Figure 4 shows the proposed target spectrometer magnet, and also indicates the target position and beam direction. The shape of the magnet poles and the position of the target reflect the three kinematic comments at the end of the last section. The magnet is made with the return yoke upbeam of the target to allow good coverage of the solid angle region which is most important, on either side, and downbeam, of the target. The beam reaches the target through a hole in the return yoke.

In setting the scale for the magnet we have tried to keep the field volume as small as possible. The mass resolution for the N* could be improved by using a larger and more expensive magnet, but for a first generation experiment we believe the proposed design is sensible. The pole tips are 0.6 m wide and 2 m long, and the gap is 0.6 m, and the return yoke cross section has been taken as 1.33 times the pole tip area. The weight of iron is about 150 tons, and the weight of copper is about 4 tons for a power requirement of 1 megawatt.

While the pole tips are shown with square corners, it will almost certainly be advantageous to shape the pole faces so that the field shape is as convenient as possible for computing particle momenta from wire chamber data. We cannot change the fact that the field of the magnet is almost all fringe field, but we hope to make it a well-behaved fringe field with 18 Kg at the pole tips.

3. Detection system

Figures 5 and 6 indicate one possible arrangement of spark

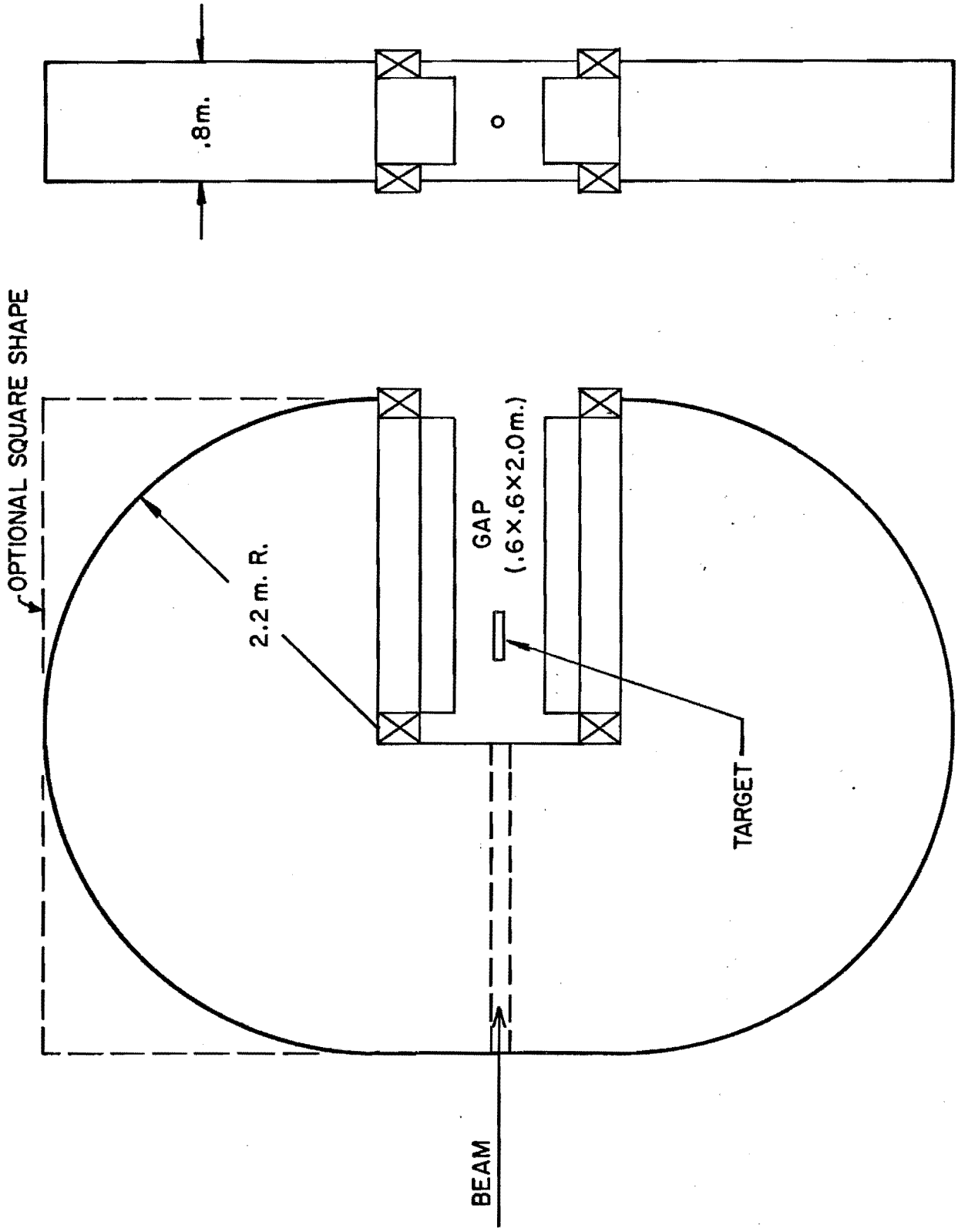

Figure 4. Sketch of the magnet for the target spectrometer.

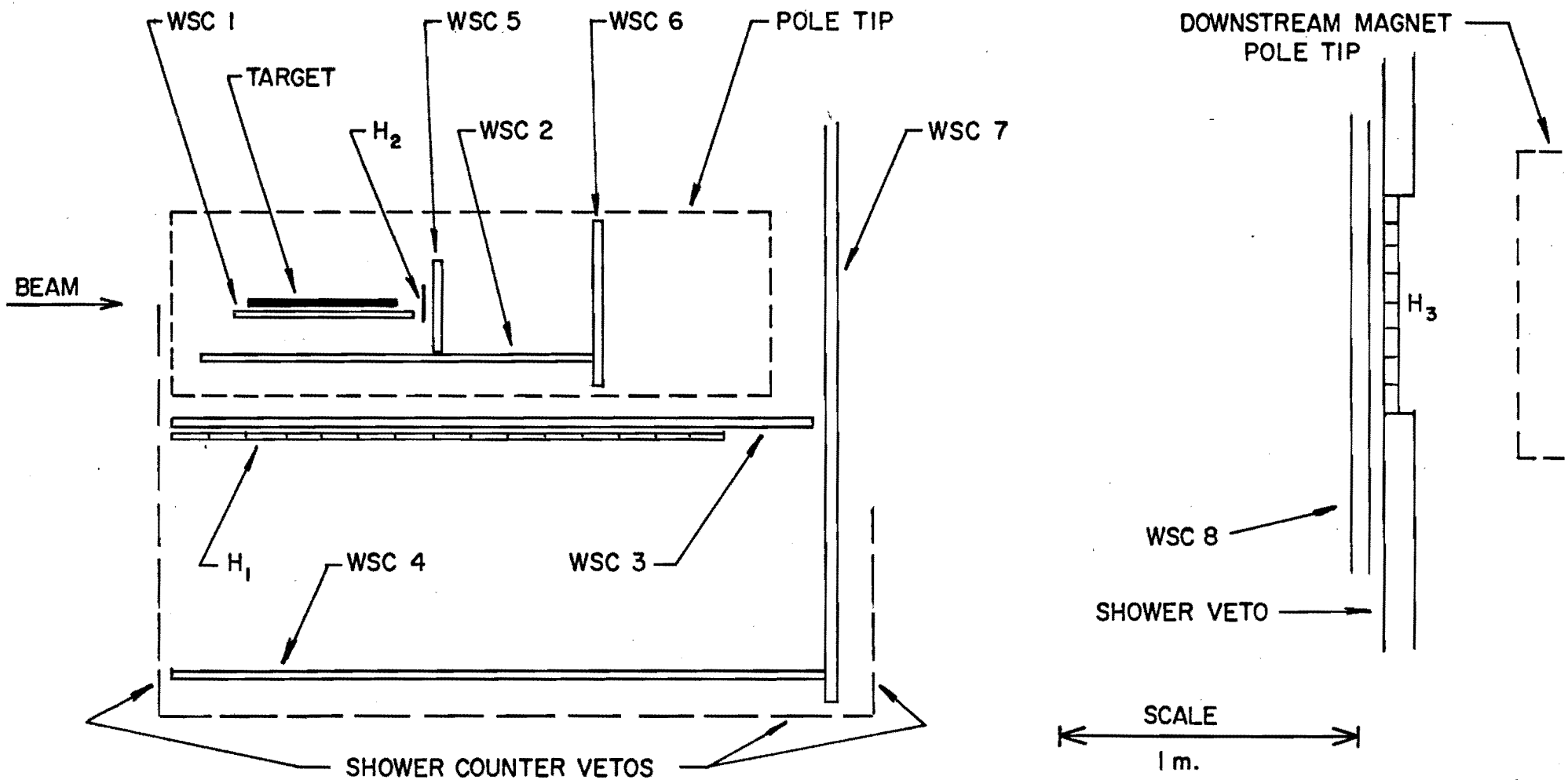

Figure 5. Plan view of the target spectrometer. Wire spark chamber planes are indicated by WSC, and hodoscopes by H. The dashed lines outline magnet poles.

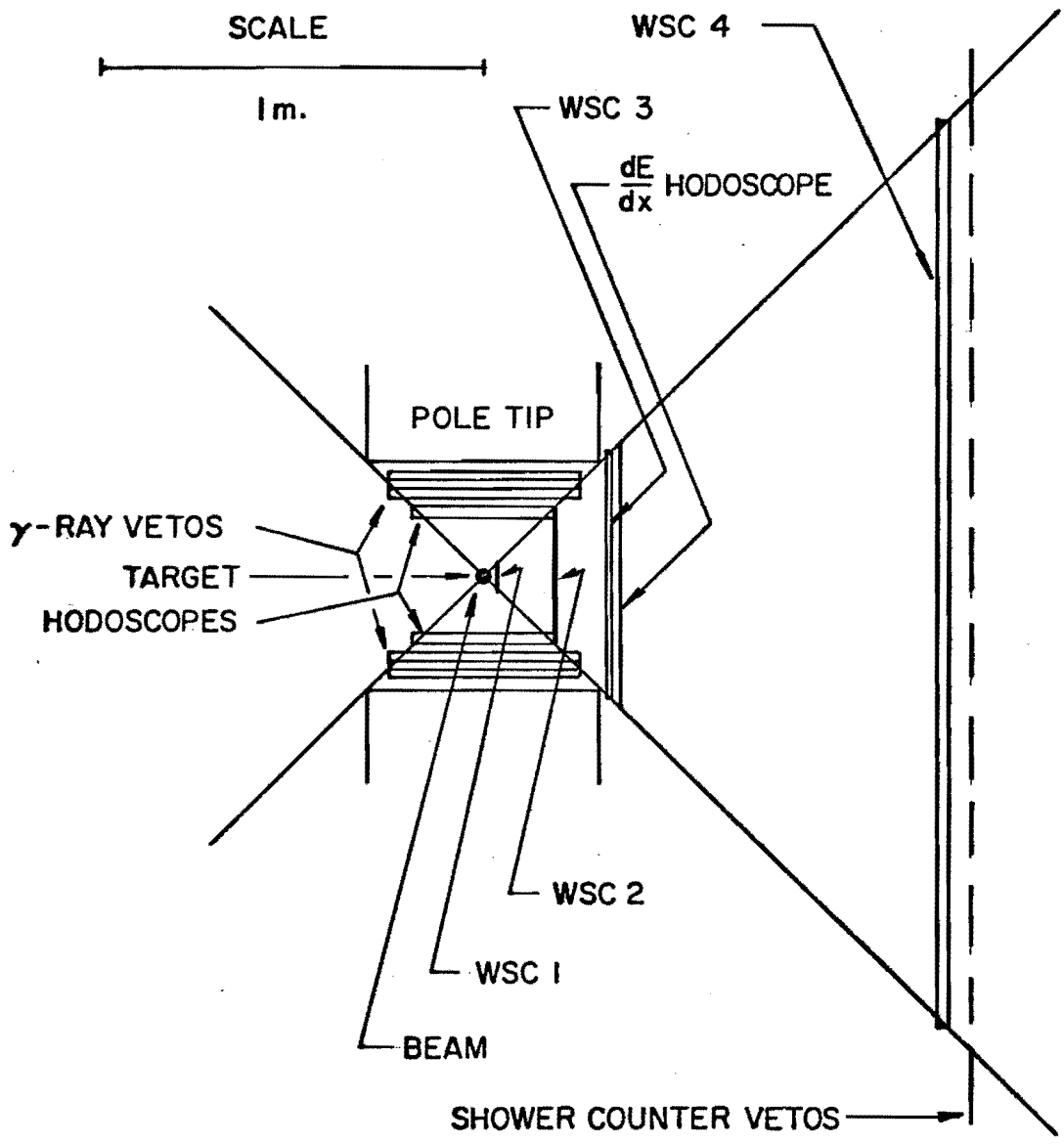

Figure 6. View along the beam line of the target spectrometer.

chambers and counters for the target region. The main requirements on this apparatus are as follows:

1) Gamma ray detectors with almost 4π solid angle, for vetoing events with slow pi zeroes.
2) Charged particle counters with 4π solid angle to determine how many charged particles are involved and to determine dE/dx for each particle.
3) Momentum measurements of the N* decay products and of slow meson-resonance decay products, over as large a solid angle as possible.
4) Position and angle measurements of fast, forward going, meson resonance products (as part of the forward spectrometer system).

In addition, the target must allow slow protons to escape as easily as possible. It is assumed that the hydrogen cell is only about 0.5 cm. in diameter, and that the total material between the hydrogen and the first spark chamber is held to a minimum (about .010" mylar, or equivalent, may be reasonable).

The gamma ray detectors will be lead-scintillator shower counters. The scintillators forming the hodoscope H1 are intended to help determine the event topology and to measure dE/dx. In some cases the dE/dx information will help distinguish protons or kaons from pions. This hodoscope is placed behind the third wire chamber plane, so that the momentum determination for slow protons will not be affected by scattering and energy loss in these counters. The remainder of the solid angle is covered by counters within the magnet gap, to

determine that event topologies are appropriate before the spark chambers are triggered.

Four planes of wire chambers are used for measuring the momentum of particles emitted between about 15 and 135 degrees in the lab. Chambers 1, 2, and 3 are for low momentum particles, while chamber 4 is useful at higher momenta, when the scintillators do not degrade the measurement and when a longer measurement base line is needed. A wire "chamber" is likely to be two or more wire planes, so that the final setup will have a degree of redundancy for checking and for resolving ambiguities.

Wire chambers 5, 6, 7, and 8 are utilized for determining momentum of forward going particles. Chambers 5, 6, and 7 will be quite adequate for the baryon resonance decays. For particles from the meson resonance which are outside the acceptance of the forward spectrometer magnet, chamber 8, in conjunction with the other target chambers, can provide useful data.

The size of the forward spectrometer is largely determined by the target to spectrometer distance required to make the highly precise angular measurement needed in the momenta of the forward going particles. To keep the size of the spectrometer to a minimum we have improved the angular resolution over standard spark chamber resolution by the use of a solid state counter hodoscope. This hodoscope labeled H2 is intended to be formed from two totally depleted surface barrier solid state counters, each with its collector plate in the form of an array of individual strips 0.2 mm. wide. Since the highest momentum particle are at small angles, the area of this

hodoscope might be 2 x 2 cm. The price of putting individual preamplifiers on each of 200 collector strips is not prohibitive, and the spatial resolution of such a device is $\pm$ 0.1 mm.

The hodoscope H5 will introduce negligible error if the standard deviation in wire chamber 8 is .3 to .5 mm., consistent with current practice. However, it is important to achieve the highest possible resolution at chamber 8, and various techniques for improving the resolution will be studied for use in this critical location. The other wire chambers are assumed to be standard chambers, with 1 mm. spacing and $\pm$ 0.4 mm. error of measurement.

4. Momentum and Mass Accuracy

The magnetic field of the target spectrometer will be assumed to be as shown in Figure 7. The results shown in this figure are for the two-dimensional problem with pole pieces in the form of circular cylinders of infinite permeability. For the present, this is an adequate beginning. As a further approximation, we will represent the B/B_o curve by two regions, each with uniform field as shown by the dashed lines on Figure 7. The field from x = 0 to x = a is taken to be B_1, and B_2 is the field for x = a to x = 3a. The average flux density at the pole tip, B_o, will be taken to be 18 kilogauss, so that B_1 is 8.5 Kg and B_2 is 2.7 Kg. We will estimate momentum resolutions by assuming that three points along the particle trajectory are determined.

Consider, as sketched below, the distance d which is a measure of the bending of a particle in two regions of lengths L_1 and L_2, with magnetic fields B_1 and B_2.

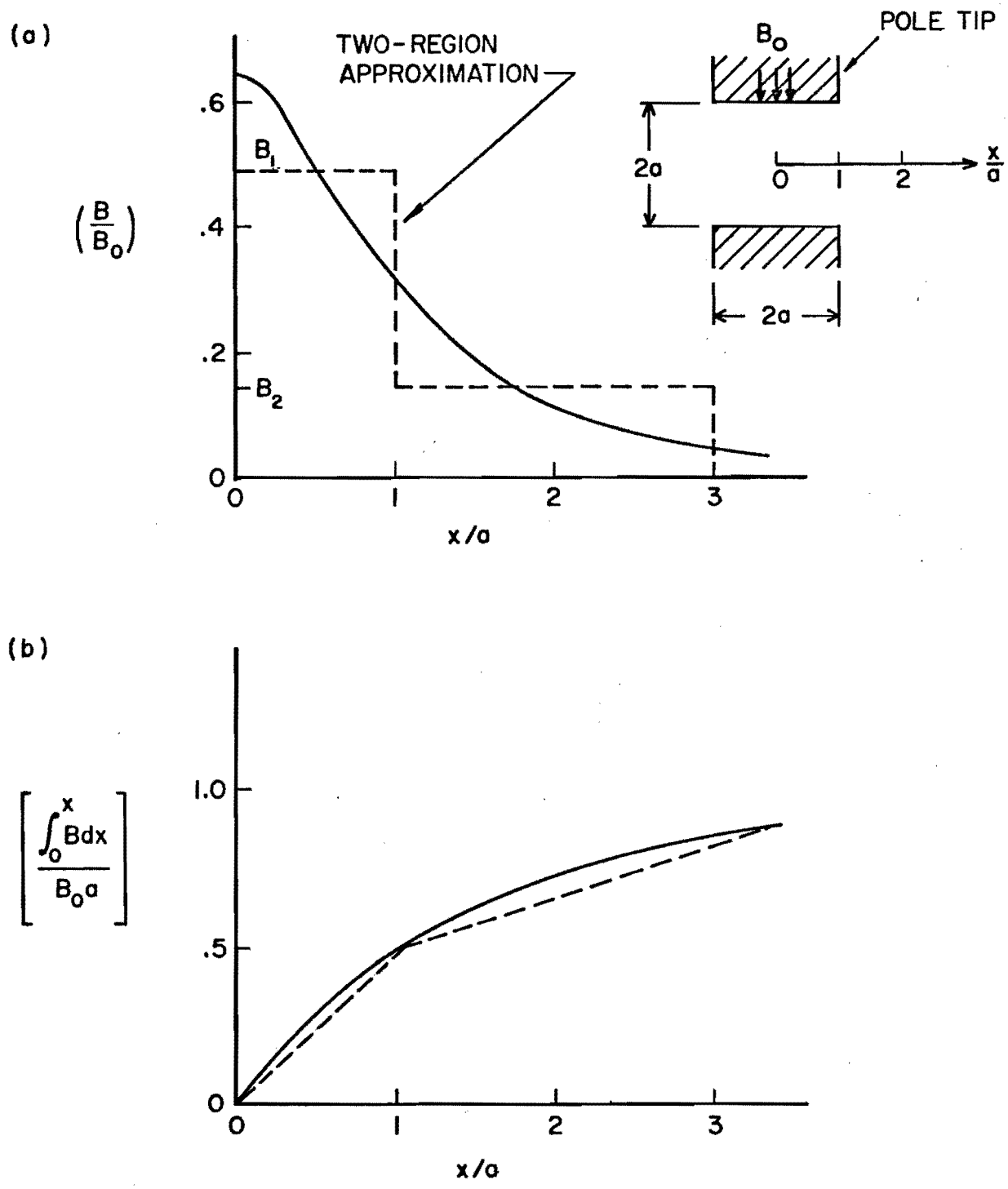

Figure 7. Model magnetic field for the target spectrometer. The solid curves are actually for pole tips in the form of infinitely permeable parallel cylinders (a two dimensional dipole field), while the dashed lines are a simple approximation used in evaluating the momentum resolution.

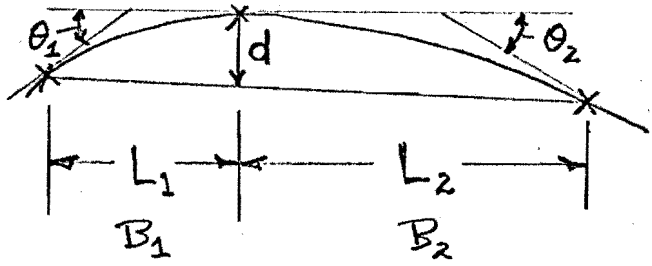

In the approximation where the bend angles θ_1 and θ_2 are small, it is easy to derive the result

$$d = \frac{150}{p}\left[\frac{L_1 L_2}{L_1 + L_2}\right](L_1 B_1 + L_2 B_2)$$

where p is in GeV/c, B is in webers/m^2, L_1 and L_2 are in meters, and d is in millimeters.

If each coordinate is known with an uncertainty ϵ_o, and these are combined like random gaussianly distributed errors, then the uncertainty in d is given by the expression:

$$\epsilon_d = \epsilon_o \sqrt{1 + \left[\frac{L_1}{L_1 + L_2}\right]^2 + \left[\frac{L_2}{L_1 + L_2}\right]^2} \ .$$

The value of $\left(\frac{\epsilon_d}{\epsilon_o}\right)$ varies within narrow limits for extreme values of the ratio L_1/L_2:

$$(\epsilon_d/\epsilon_o)_{min} = 1.22 \qquad L_1 = L_2;$$

$$(\epsilon_d/\epsilon_o)_{max} = 1.41 \qquad L_1 \gg L_2,\ L_2 \gg L_1 \ .$$

At each wire plane we will assume an uncertainty of $\pm$ 0.4 mm., representative of good current wire spark chamber performance. At a laboratory angle of 90 degrees, the uncertainty in momentum for

wire chambers 1, 2, and 3 is estimated to be

$$\left(\frac{\Delta p}{p}\right)_{123} = \delta_{123} = \pm\ 0.17\ p, \text{ with p in GeV/c .}$$

For the 90 degree case we can also consider a three point measurement involving chambers 1, 3, and 4. The longer baseline and greater field integral help a great deal, giving an offset distanced about six times greater than in the first case. For chambers 1, 3, and 4 the error is

$$\left(\frac{\Delta p}{p}\right)_{134} = \delta_{134} = 0.030\ p, \text{ with p in GeV/c.}$$

For particles with directions other than 90 degrees, the path length in the field increases, and the spark chamber errors also increase because of the non-normal trajectories. However, at angles of 30-45 degrees in the lab we expect a net imporvement of about a factor 2 compared to the errors noted above.

For particles at angles between 0 and 15 degrees, chambers 5, 6, and 7 are assumed to operate in a uniform field equal to B_1, leading to an uncertainty

$$\delta_{567} = 0.010\ p,\ p \text{ in GeV/c.}$$

For forward particles which reach chamber 8, the error is reduced by a factor of about 3 to

$$\delta_{578} = 0.0038\ p, \text{ with p in GeV/c.}$$

Thus far we have ignored any degradation in the momentum reso-

lution due to multiple scattering. For measurements involving the forward wire chambers 5, 6, 7, and 8 the multiple scattering is not important because of the greater path length in the magnetic field and the generally high particle momenta.

For measurements involving the system consisting of chambers 1, 2, and 3, the dominant effect of multiple scattering comes from the material of chamber 2. For measurements with chambers 1, 3, and 4, the dominant effect comes from the counter hodoscope behind chamber 3.

We will assume that chamber 2 scatters like 1.6×10^{-3} radiation length (about .025" of plastic), while the hodoscope scatters like 2.5×10^{-2} r.l. (about 1 cm. of plastic). For pions, the multiple scattering errors are as follows

$$(\delta_{123})_{\text{rms}} = .015$$

$$(\delta_{134})_{\text{rms}} = .030 ,$$

while for protons, with lower velocities the errors are larger. For 300 MeV/c, 500 MeV/c, and 1000 MeV/c protons the errors are as follows:

	300 MeV/c	500 MeV/c	1000 MeV/c
(δ_{123})	.05	.03	.02
(δ_{134})	.10	.06	.04

Depending upon the momentum, the multiple scattering or the geometrical uncertainties in the momentum determination may be most

important. Figure 8 shows the net estimated momentum uncertainties for the (1, 2, 3) and (1, 3, 4) determinations at lab angles near 90 degrees.

Figure 8 shows that for a large range of momentum, up to about 2 GeV/c, the relative momentum error is about 5%. A rough guess would be that the Q value of a two body decay into particles of momentum < 2 GeV/c could then be determined to about this accuracy. A detailed study of the examples shown in Figures 1 and 2 has confirmed this expectation. The average mass resolutions found were 6% and 4% of the Q-values:

For N^*_{1238}; $\Delta M \approx \pm$ 10 MeV; and for

N^*_{2000}; $\Delta M \approx \pm$ 40 MeV.

Furthermore, the resolutions are only weakly dependent upon the N* decay angle in its rest frame or on the t values.

In the estimates of mass resolution, we have included multiple scattering in the target and wire chambers, inasmuch as it leads to an uncertainty in the angle between the two decay products, which leads to a mass uncertainty. However, the effect of this scattering is negligible, because it is only severe for low momentum protons whose influence on the mass is minor.

For a pion-proton system the mass determination depends upon correctly identifying the pion and proton when their lab momenta are significantly different. In this case, their lab angles enable the identification to be made unambiguously. Of course, for $p\pi^-$

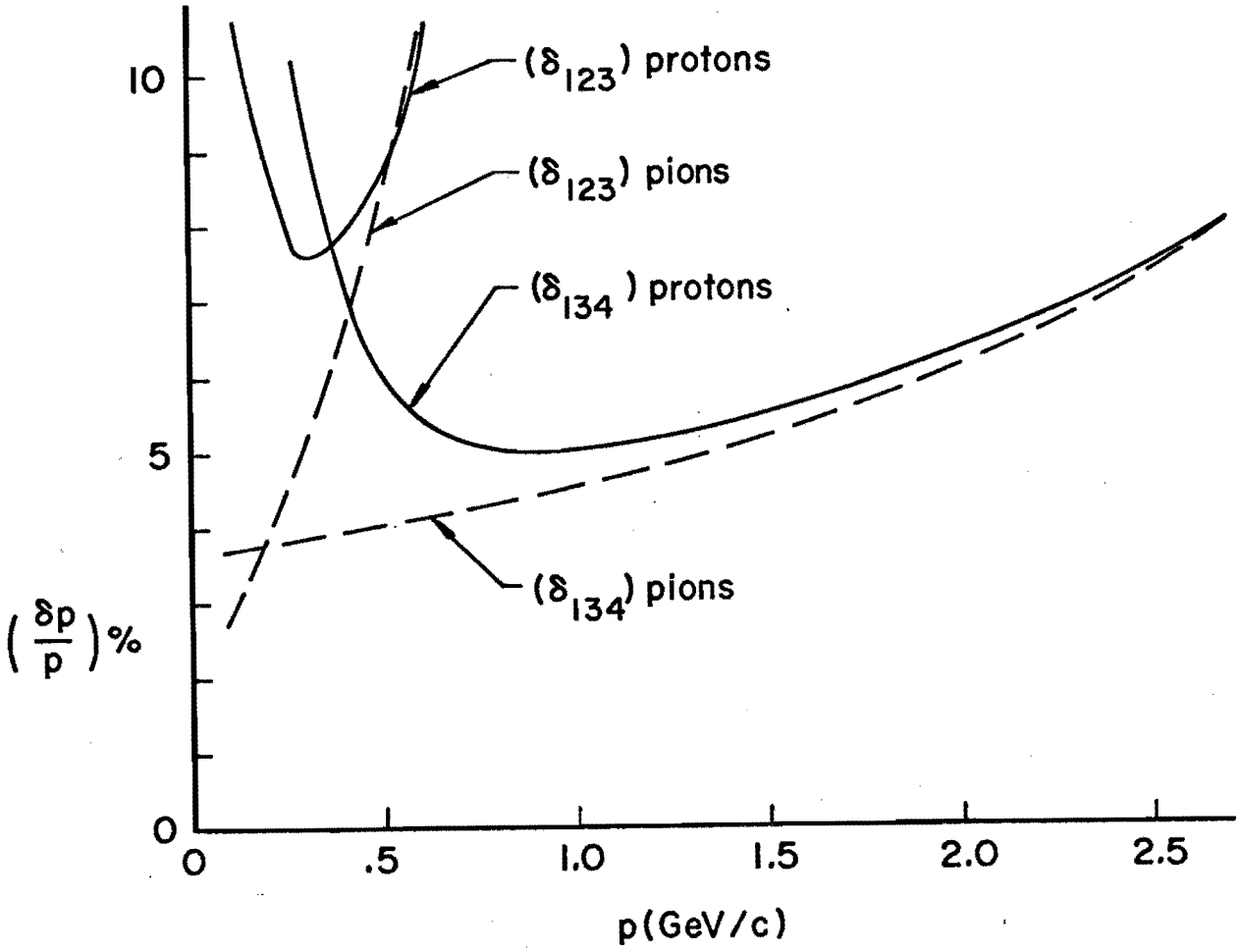

Figure 8. Estimated momentum resolution for the target spectrometer. The fractional error (δ p/p) is given as a function of p for particles moving at 90° in the laboratory (which is the worst case). Results are shown for spark chambers 1, 2, and 3 and for chambers 1, 3, and 4.

states the charge immediately determines the particle identities. The dE/dx information from the scintillation counters will be most important for distinguishing πp from $\pi\pi$ states and for distinguishing Kp from πp states in favorable cases.

C. Forward Spectrometer

Figure 9 shows a plan view of the forward spectrometer. We intend to accurately measure the momentum of particles emitted between zero and 30 degrees, taking account of the fact that high momentum particles from meson resonances with mass up to about 4 GeV are mainly contained in a narrow 5 degree cone. Figure 10 shows the kinematics for ρ^{o} decay and for the 3π decays: $X \rightarrow \pi\rho$. We will defer consideration of the three-body final states until the end of this section and emphasize the two pion decays first. The $\pi\rho$ kinematics are essentially identical to $\pi\pi$ kinematics for masses of 2, 4, and 6 GeV.

The forward spectrometer magnet is intended to be a standard H-magnet, with pole tips two meters long and one meter wide. We have assumed a gap of 0.5 meters and a field of 18 kilogauss. At a sacrifice in counting rate, but not in any other important respect, the magnet gap could be reduced. For high momenta, the spectrometer utilizes the forward magnet and wire chambers 5, 8, 9, and 10. The solid state hodoscope H2 is expected to provide better spatial resolution than chamber 5, but in what follows we leave this as a factor of safety.

For moderate momenta, chambers 5, 8, and 9 provide good accuracy, while the target spectrometer magnet and chambers 5, 7, and 8 are used for particles which miss the forward spectrometer aperture. If an accuracy of $\pm$ 0.5 mm. is assumed for all wire chambers, then the momentum errors for various combinations of wire chambers are as follows (with p in GeV/c):

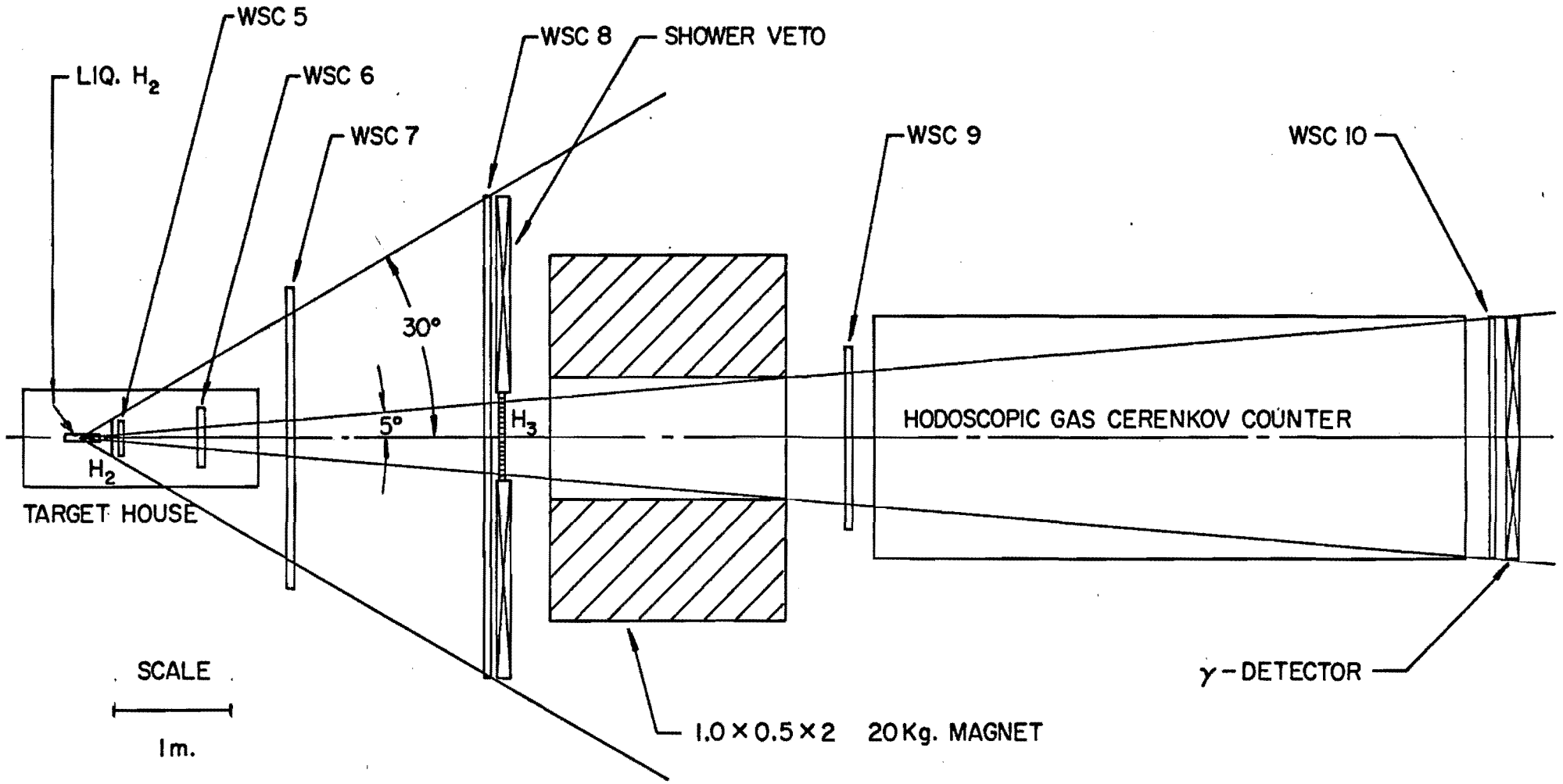

FORWARD SPECTROMETER

Figure 9. Plan view of the forward spectrometer. Wire spark chamber planes are labeled WSC and hodoscopes are labeled H.

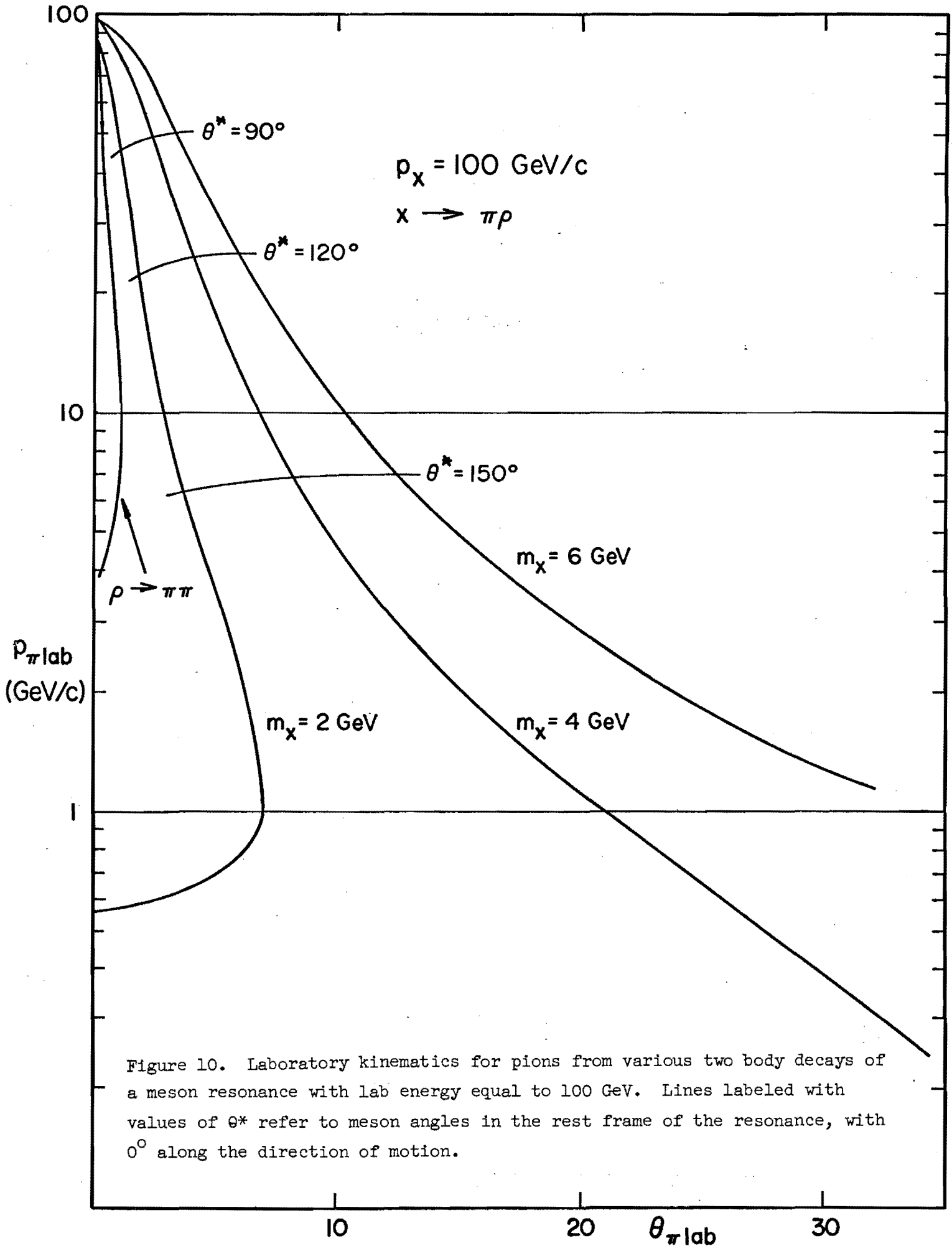

Figure 10. Laboratory kinematics for pions from various two body decays of a meson resonance with lab energy equal to 100 GeV. Lines labeled with values of θ^* refer to meson angles in the rest frame of the resonance, with 0° along the direction of motion.

$$\delta_{5,7,8} = (0.35\ p)\%$$

$$\delta_{5,8,9} = (0.068\ p)\%$$

$$\delta_{5,8,9,10} = (0.013\ p)\%$$

For a two body decay, the mass is given by the following formula:

$$M_x^2 = M_1^2 + M_2^2 + 2(E_1E_2 - p_1p_2 \cos \theta_{12}),$$

or approximately:

$$M_x^2 \quad p_1p_2\,\theta_{12}^2\ ,\ \text{for}\ \theta \ll 1,\ M_x^2 \gg M_1^2,\ M_2^2;\ p_1 \gg M_1;\ p_2 \gg m_2^1$$

The mass uncertainty in the small angle case is quite simple:

$$\left(\frac{\Delta M_x}{M_x}\right) = \left[\frac{1}{4}\left\{\left(\frac{\Delta p_1}{p_1}\right)^2 + \left(\frac{\Delta p_2}{p_2}\right)^2\right\} + \left(\frac{\Delta\theta}{\theta}\right)^2\right]^{1/2}$$

Figure 11 shows the general result for $\frac{\Delta M_x}{M_x}$ and indicates that the small angle formula gives a good estimate over the entire region of interest here.

Typical mass resolutions which will be attained with this spectrometer have been evaluated assuming the pion momenta are in the ratio 2:1. They are as follows:

M_x	$(\Delta M_x/M_x)$	ΔM_x
.75 MeV	1.3%	10 MeV
2.0 MeV	0.9%	18 MeV
4.0 MeV	0.7%	28 MeV

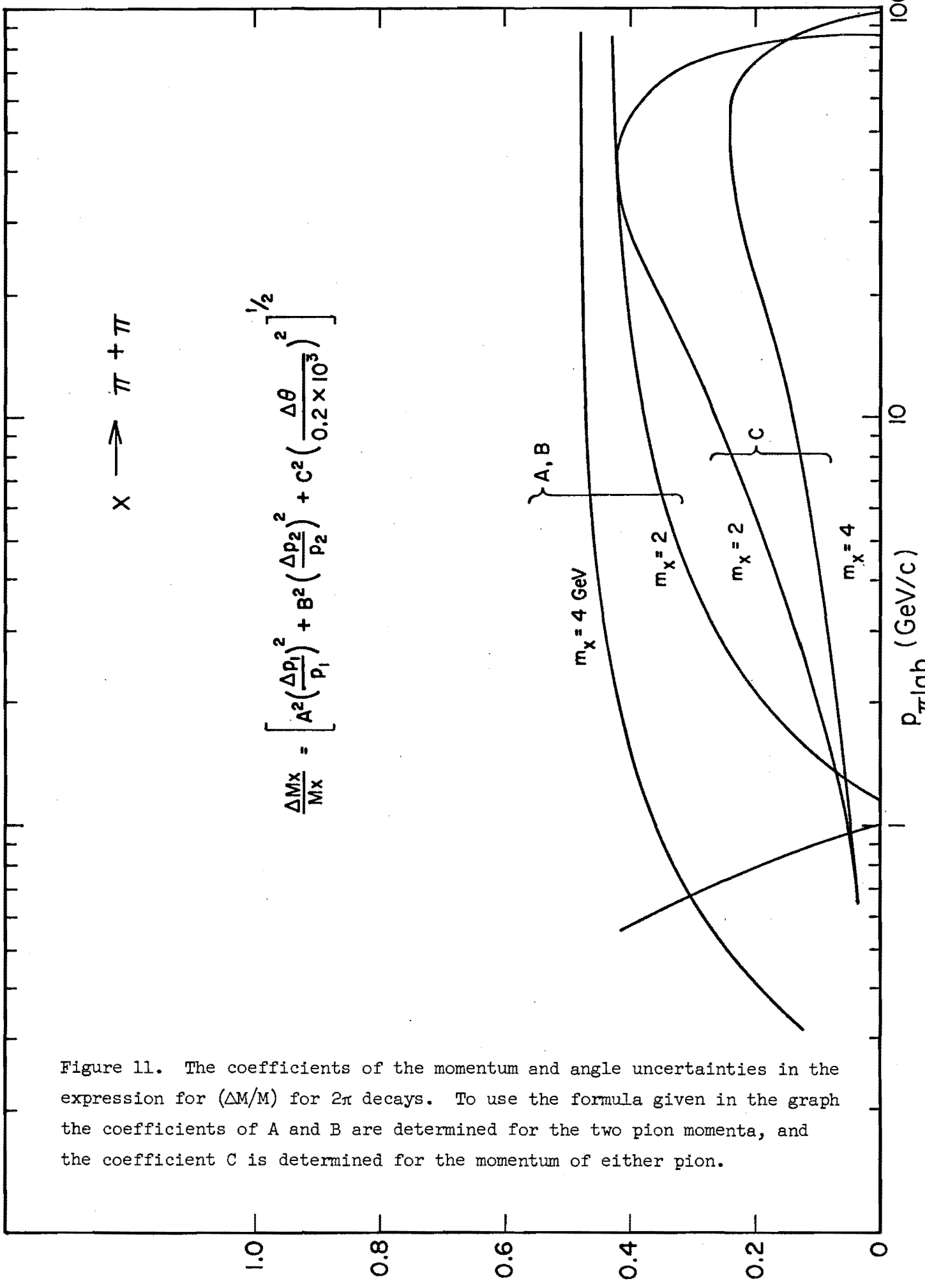

Figure 11. The coefficients of the momentum and angle uncertainties in the expression for $(\Delta M/M)$ for 2π decays. To use the formula given in the graph the coefficients of A and B are determined for the two pion momenta, and the coefficient C is determined for the momentum of either pion.

These mass resolutions are valid for any case where both decay mesons enter the forward spectrometer magnet. For mesons outside this aperture with momentum less than about 5 GeV/c, the estimates are still good. Thus, referring to the kinematics shown in Figure 10, for masses up to about 2 GeV the good resolution applies to the entire range of decay angles in the M_x cm. system. At higher masses, part of the available solid angle suffers from reduced mass resolution, but up to a mass of 4 GeV less than half the total solid angle is affected.

This concludes our discussion of the two pion decays. For the three pion decays the situation is much more complicated, especially if one of the pions is neutral. We dismiss the charged pion case as not appreciably different from the two pion case except for some reduction in useful solid angle. For the case of two charged pions and one neutral pion, the case of symmetric 3-body decay at 90 degrees in the cm. system has been taken as typical. The mass resolutions are as follows:

M_x	$\frac{\Delta M_x}{M_x}$	ΔM
0.78 MeV	(6.7)%	52 MeV
2.0 MeV	2.0%	40 MeV
4.0 MeV	1.8%	72 MeV

The calculation in this case involves utilizing the observed transverse momentum of the charged pions, or a knowledge of which gamma ray is more energetic, to remove the ambiguity in determining the meson direction from the gamma ray directions. For very low masses the resolution becomes particularly poor. The decay geometry for which the resolutions were cal-

culated is neither the most favorable nor the worst, so these are representative values, subject to variation by at least a factor of 2 over the range of possible decay kinematics.

D. Gas Cerenkov Counter

The general layout of this counter is shown in Figure 12. It consists of a 10 meter long gas radiator, a 3 meter by 1.5 meter concave mirror and eight 2" photomultipliers. All the light produced by particles with a momentum higher than 10 GeV/c and within the production cone accepted by the forward spectrometer is focused on an area 26 cm. x 3 cm. The optics are arranged in such a way that there is a fairly good correlation between the particle momentum, its charge (sign), and the position on the photomultiplier plane where the light is focused. This arrangement permits the simultaneous and independent measurement of the Cerenkov light produced by two particles with opposite charge, or with the same sign of charge, but significantly different momentum (20 GeV/c and 40 GeV/c, for example).

The n-1 (index of refraction minus one) for the radiator is 10^{-4} for a pion threshold of 10 GeV/c and 4.5×10^{-5} for a threshold of 15 GeV/c. These low indexes will be obtained by using a mixture of helium and argon at atmospheric pressure, so that the gas container only has to be light tight but does not have to have any significant mechanical strength. The 3 meter by 1.5 meter concave mirror will be made as a mosaic of smaller front surface plane mirrors.

In order to work comfortably down to the one photoelectron level, we will use RCA C31000D photomultipliers. These tubes, with their high-gain first dynode, have extremely low dark current (~800 counts/minute at 1/20 single photoelectron output), and their ability to distinguish between one, two and three photoelectrons provides a very reliable self-calibration of the system.

In order to estimate the performance of the counter the Cerenkov light spectrum has been folded over the published response of the RCA C31000D photomultiplier. From this calculation, and from the usual theory of Cerenkov emission, we can write the following formula for N, the number of photons per meter:

$$N = 10^4 \left[\left(\frac{m_t}{p_t} \right)^2 - \left(\frac{m}{p} \right)^2 \right] \text{ p.c./m.}$$

The quantities p_t and m_t represent the threshold condition for which the counter is adjusted, with p_t and m_t the momentum and mass of a particle at threshold. The ratio (p_t/m_t) determines the maximum photon yield per meter N_{max}, the index of refraction n, and the maximum Cerenkov angle according to the formulas below.

$$N_{max} = 10^4 \left(\frac{m_t}{p_t} \right)^2 \; ; \quad (n-1) = \frac{1}{2} \left(\frac{m_t}{p_t} \right)^2 \; ; \quad \theta_{max} = \frac{m_t}{p_t}$$

At 100 GeV/c, a reasonable operating point for the counter is with the threshold at 15 GeV for pions. Figure 13 shows the number of photoelectrons as a function of pion and kaon momentum for this case. The π - K separation becomes most difficult at high momentum, and Figure 14 shows the differential and integral photoelectron distributions at 70 and 80 GeV/c. The integral probabilities are for greater than the indicated number of photoelectrons for pions and less than the number of photoelectrons for kaons.

In discussing threshold pulse height criteria for the counter, we envision establishing the criteria after the wire chambers have been triggered,

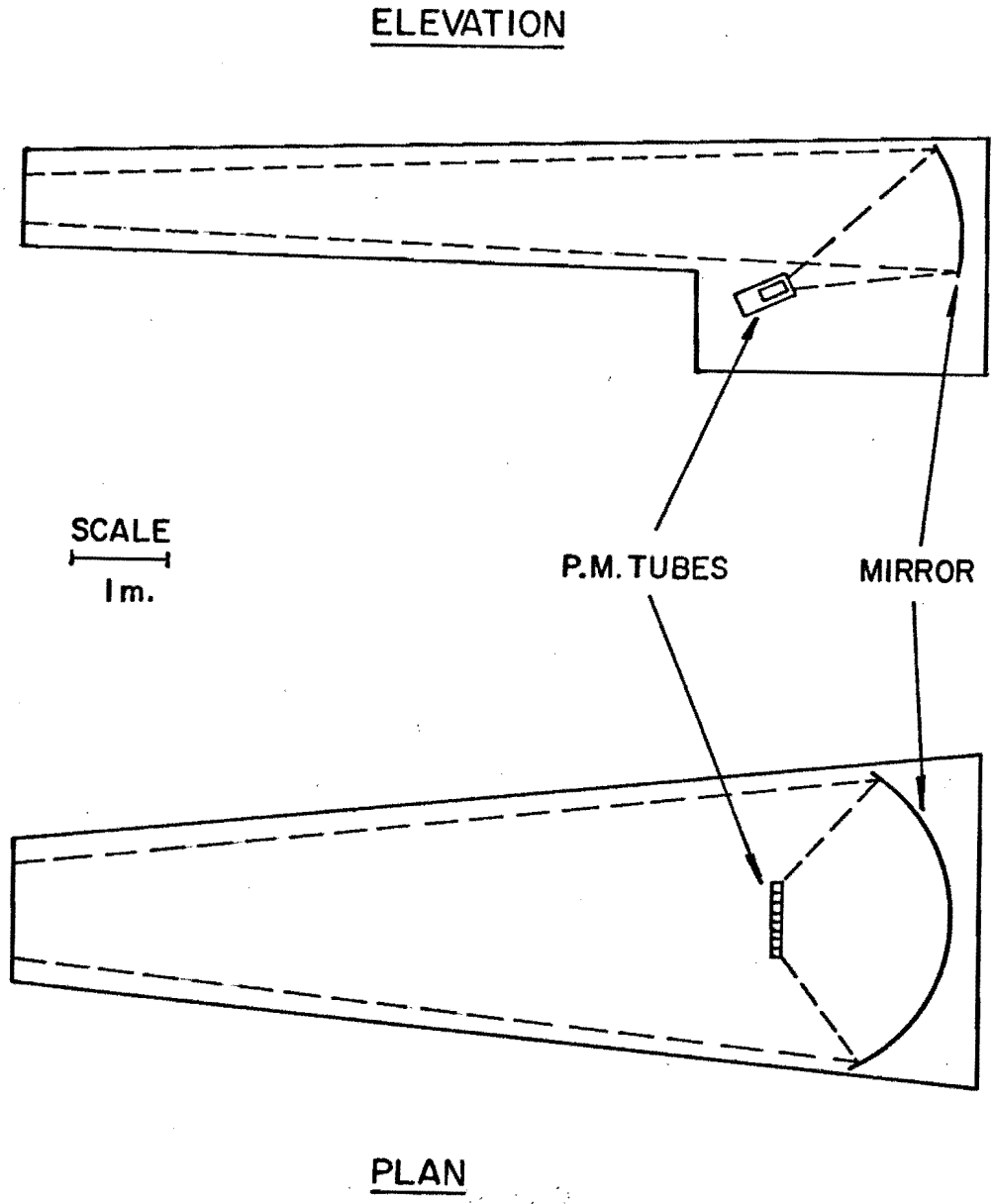

Figure 12. Schematic view of the gas Cerenkov counter. The beam direction is from left to right on the figure. The large mirror is actually a mosaic of smaller plane mirrors.

Figure 13. Number of photoelectrons for the gas Cerenkov counter as a function of momentum, with the refractive index of the gas adjusted so that threshold for pions is 15 GeV/c.

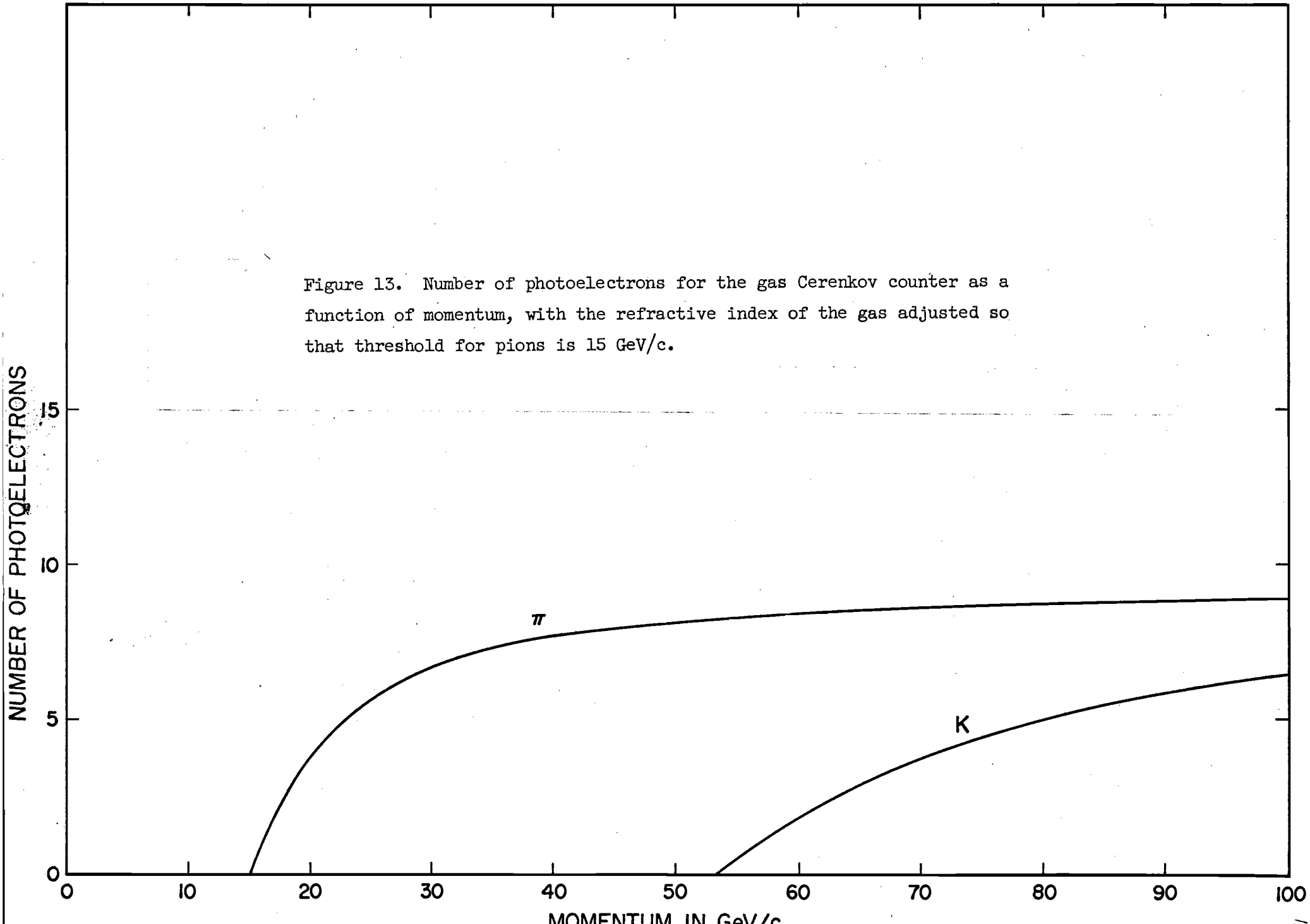

Figure 14. Differential and integral distributions of N, the number of photoelectrons from the gas Cerenkov counter, for pions and kaons at 70 and 80 GeV/c. The counter is assumed to operate at a pion threshold of 15 GeV/c.

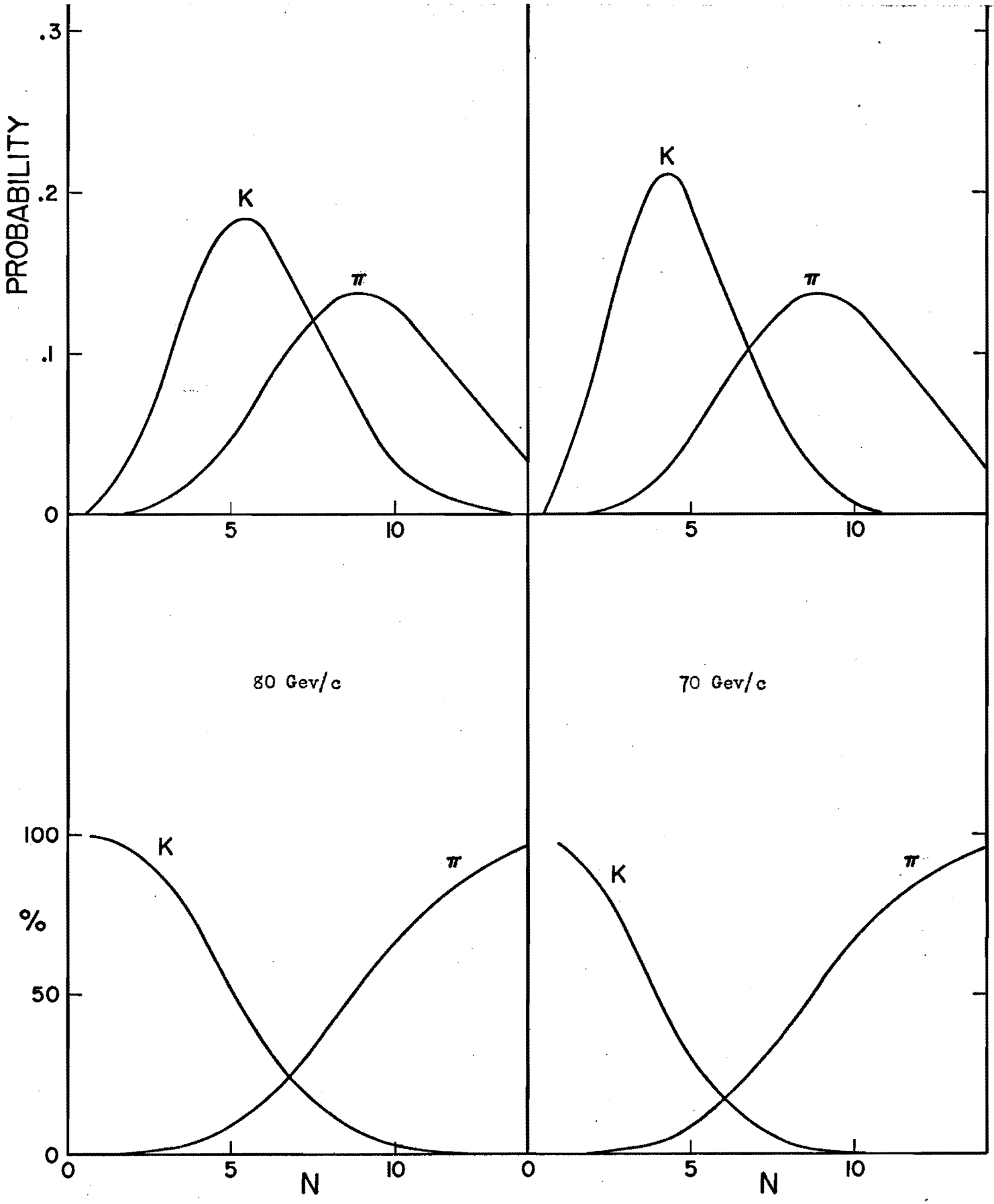

so that momentum-dependent criteria are possible. Furthermore, the pulse height will be recorded for each phototube, so that different criteria can be set depending on the purpose of the data analysis.

If it is desired to select pions, Figure 14 shows that a threshold of 9 photoelectrons at 80 GeV/c gives 55% pion efficiency and 6% kaon efficiency. Even at this high momentum the counter performs usefully, and of course the π-K separation becomes much better for lower values of momentum. Pulse height criteria can confidently be established with good precision, because for momenta between pion and kaon threshold the Cerenkov light is known to come from pions. The response of the detector is therefore continuously calibrated by pions over a wide range of particle trajectories during the data collection.

There are three types of two-meson combinations which the counter is intended to identify: π-π, π-K, and K-K. To select π-π events the threshold will be set low below the momentum which corresponds to K-threshold, and relatively high above this momentum, to minimize the chance that a K appears to be a π. For the π-K state the threshold at momentum above K-threshold should be set relatively low, to minimize a chance that a pion is identified as a kaon.

The table below gives examples of the relative efficiency for recording some two-body resonances if momentum and pulse height criteria are applied so that the Cerenkov counter gives a ratio of 10:1 or better for detection of wanted vs unwanted particles. The efficiencies are calculated for an isotropic decay distribution of the two-meson state.

	$\pi\pi$	$K\pi$	KK
ρ	60%	-	-
K* (890)	-	60%	-
Φ	-	-	100%
Mass = 2000	60%	40%	40%

In order to distinguish protons from kaons, the counter must be run at a higher index of refraction, which is accessible without exceeding a pressure of one atmosphere. Good separation can be obtained for a wide range of proton momentum. The index also must be raised, for beam momenta below 100 GeV/c, and the counter performs better because of better photon statistics. The photon statistics become worse at higher momentum, assuming counter operation with correspondingly higher pion threshold. However, for extensive running at momenta near 200 GeV/c it will be possible to double the length of the counter, since the important region of forward solid angle is about half that for 100 GeV/c. For distinguishing protons from mesons near 200 GeV/c, the standard 10 meter configuration works quite well.

IV. Run Plan

A. Beam Intensity

The maximum beam intensity is determined either by the allowed accidental rate of old tracks in the spark chambers or by the available beam, whichever is lower. In calculating the accidental rate we have made the following assumptions:

1. a spark chamber sensitive time of 2 microseconds;
2. a total p-p cross section of 40 mb.;
3. a total π-p cross section of 25 mb.;
4. an acceptable accidental probability of 10%;
5. a beam spill length of 1 second.

As a prototype beam, we have used the 2.5 mrad beam described by Reeder and MacLachlan in the 1969 Summer Study report SS-41. We have assumed beam intensities per pulse as given in that report, for 3×10^{12} protons on target, subject to the accidental rate limitation. The beam momentum spread has been taken as 0.5%. The table below lists the resulting intensities.

Beam Intensity per Pulse

Energy	Sign	p	π	K
50 GeV	+	$.7 \times 10^6$	2×10^6	$.8 \times 10^5$
	-	2×10^4	2×10^6	3×10^4
100 GeV	+	1.2×10^6	2.6×10^6	2.1×10^4
	-	$.7 \times 10^4$	2×10^6	2×10^4
150 GeV	+	1.2×10^6	$.6 \times 10^4$	2×10^3
	-	-	$.5 \times 10^6$	$.5 \times 10^4$

For an arbitrary cross section of one microbarn, the beam intensities of the preceding table have been converted to event rates. A target length of 30 cm. and an overall detection efficiency of 10% (which we believe is conservative) were assumed. The table below gives the resulting rates.

Event Rates per Hour

(1 μb cross section and 10% detection efficiency.)

Energy	Sign	p	π	K
50	+	50	140	60
	-	1.4	140	2.0
100	+	800	18	1.5
	-	.5	140	1.4
150	+	800	.42	.14
	-	-	35	.35

B. Run Plan

The equipment can be operated in the following modes:

1. Beam polarity $\pm$
2. Cerenkov index of refraction set for π-Kp or πK-p discrimination denoted by π mode or p mode (as discussed in Section II-D).
3. Trigger electronics set for diffractive or non-diffractive processes, denoted by D or $\not{D}$ (as discussed in Section II-A).

A short description of each mode now follows:

$\pm$ π $\not{D}$ - This is expected to be the main mode of operation, from which the bulk of the physics is presently expected to come.

$\pm$ p $\not{D}$ - This mode, in which protons are distinguished from mesons, has a dual purpose: to study baryon exchange reactions and pp states, and to evaluate backgrounds from forward baryons in the πK and KK data taken in the preceding mode.

$\pm$ π D - In this mode we will study π-p diffractive processes which are expected to have much higher cross sections than the other reactions of interest.

$\pm$ p D - In this mode we will study p-p and $\bar{p}$-p diffractive processes.

One of the most important aspects of the proposed experiment is that the physics results will be available on line. Since we can hardly predict with certainty what we will find, a run plan formulated at this time is a first guess, subject to change as soon as preliminary data is available.

Table I gives cross section estimates for processes that are typical of the ones we want to measure. Available data at the highest energy has been extrapolated to higher energy as a power of lab beam momentum. It seems from this table that a reasonable preliminary goal is to obtain a few thousand events per microbarn cross section (except for events from incident K's). A proposed run plan for the various modes of operation as well as various beam energies is given in Table II.

Table 1

Measured Cross Sections Extrapolated to Incident Momenta of 50,100,150 GeV/c

Reaction	$\sigma(p^{lab})$ μb	p^{lab}	n^*	σ(50 GeV/c)	σ(100 GeV/c)	σ(150 GeV/c)
PI+ P GT PI+ PI- DELTA++	400.00	18.50	2.00	54.76	13.69	3.42
PI+ P GT RH0 0 DELTA++	103.00	18.50	2.00	14.10	3.53	.88
PI+ P GT F DELTA++	180.00	18.50	2.00	24.64	6.16	1.54
PI+ P GT PI+ PI- PI0 DELTA++	220.00	18.50	2.00	30.12	7.53	1.88
PI+ P GT ETA DELTA++	34.00	18.50	2.00	1.77	.44	.11
PI+ P GT OMEGA DELTA++	13.00	18.50	2.00	1.78	.44	.11
PI+ P GT A1 P	140.00	18.50	.00	140.00	140.00	140.00
PI+ P GT DELTA++(FOR) RH0 0	2.00	16.00	3.00	.07	.01	.00
PI- P GT PI+ PI- DELTA++	320.00	8.00	2.00	8.19	2.05	.51
PI- P GT PI- PI- PI0 DELTA++	190.00	8.00	2.00	4.86	1.22	.30
PI- P GT PI+ PI- N*(ALL)	190.00	13.00	2.00	12.84	3.21	.80
PI- P GT PI+ PI- DELTA 0	50.00	13.00	2.00	3.38	.84	.21
PI- P GT RH00 DELTA 0	28.00	8.00	2.00	.72	.18	.04
PI- P GT K0 LAMBDA	20.00	10.00	1.80	.24	.07	.02
K- P GT PI0 LAMBDA	100.00	3.50	1.80	.56	.16	.05

* The measured cross sections listed in the first column are scaled to 50, 100 and 150 GeV/c by $(p^{lab})^{-n}$.

Table II

Proposed Running Plan (time in hours)

Energy	Mode							
	+ π D	+ P D	+ π $\not{D}$	+ P $\not{D}$	- π D	- P D	- π $\not{D}$	- P $\not{D}$
50	3	3	30	3	2	2	20	2
100	10	10	100	10	10	10	100	10
150	5	5	25	25	10	10	100	10

Total number of hours: 515.

Table III

Number of events collected corresponding to the running plan in Table II.

Energy	Beam	+ π D (1 mb)	+ P D (1 mb)	+π Ø (1 μb)	+ P Ø (1 μb)	− π D (1 mb)	− P D (1 mb)	− π Ø (1 μb)	− P Ø (1 μb)
50 GeV	p	15K (1)	15K (1)	1500	150	1400 (1)	2800	28	----
	π	15K (1)	? (2)	4200	420	14K (1)	?	2800	280
	K	15K (1)	----	1800	180	2K (1)	----	40	4
100 GeV	p	28K (2)	28K (2)	80K	8K	----	5000	500	----
	π	28K (2)	?	1800	180	28K (2)	?	14K	1400
	K	9K (6)	----	150	15	11K (8)	----	1400	140
150 GeV	p	14K (1)	14K	20K	20K	----	----	----	----
	π	1600 (2)	?	10	10	14K (1)	?	3500	350
	K	280 (2)	----	3.5	3.5	3100 (9)	----	35	3.5

* In these cases the trigger will be saturated. We have arbitrarily chosen to run on each particle the number of hours shown in parenthesis under the number of events.

The number of events for the various modes, beam particle types, and energies is given in Table III. For the diffractive mode of operation the number of events per millibarn is given, while for the non-diffractive the number of events per microbarn is given.

We estimate that a 30% overhead has to be added to the data taking time. This overhead takes care of the time required to charge operation conditions, checks and failures. A setup and testing time of four weeks running with reduced beam intensity in a parasitic fashion is also requested.

Summarizing the time requested we have:

Setup and testing	200 hours (over four weeks)
Data taking	515 hours
Overhead	150 hours

C. Data Analysis

A Sigma 2 computer will be used to read in and analyze data from the target house and the forward spectrometer. The software and hardware for this computer is presently being developed for use in a hybrid bubble, wire chamber experiment approved for running this year at SLAC. The present configuration of the Caltech Sigma 2 system is:

(a) 20K core memory with the last 4K having an external port

(b) Random access disk with a .75 M byte capacity

(c) 2 seven track tape drives

(d) 400 cpm card reader

(e) 250 lpm line printer

(f) CRT display with vector and character generator

(g) 16 priority interrupts

(h) Interface to electronics for 12 wire chambers.

The priority interrupts are essential for real time control of the experiment. The external memory port will allow for rapid transfer of data into the computer.

In order to estimate the on-line analysis capability of the Sigma 2, we review some of the relevant time intervals set by the apparatus and the accelerator. Our wire chamber system is capable of accepting 1 event every 50 ms. Over the duration of the beam spill we typically expect to accumulate approximately 10 events. There is an additional 4 sec. between the end of a beam spill and the start of the next. Within this framework we feel that the following analysis will be possible.

a. During the 50 ms interval between events, data from the counter hodoscopes, wire chambers and Cerenkov will be readout. Based on our

estimates of time requirements in the hybrid experiments we feel that 15 ms will be sufficient time to determine the mass and momentum of the forward going system with good precision. It should therefore be possible to have on-line information about the momentum and mass of the forward going system for each event. This will be an important feature of this experiment inasmuch as we anticipate a large amount of data on various reactions, which will make the conventional analysis of multiparticle reaction (geometry reconstruction and kinematic fitting) prohibitive. This information will allow us to select only events of interest for further analysis.

b. We will attempt to measure the momentum of the target house particles for at least a limited sample of the data. It is difficult to estimate the time requirement to measure the particle trajectories through a highly non-uniform magnetic field. If the time estimates for the forward particle measurements are correct, we will have about 3.5 sec to make a momentum measurement of the two particles in the spectrometer for at least one event in ten. This would permit a 10% sampling of the data while the experiment is in progress. This will be important in making decisions about the run plan of the experiment while it still is in progress.

Finally we note that other facilities will be available to do off-line analysis of the data in a more refined fashion. These are the IBM 360/44 and 360/75 at Caltech and the IBM 360/91 at UCLA.

IV. Equipment Required

We propose to provide all the experimental equipment for this experiment except for the two magnets, the hydrogen target and the Cerenkov counters associated with the identification of the beam particles. Caltech will furnish all the electronics, spark chambers and computer system; UCLA and Caltech will assume the responsibility for the hodoscope counters.

A list and short description of the main items furnished by us follows.

1. Counters

   a) Scintillation hodoscope

      H_1 2 x (.75 m x 2.5 m) use 20 - 2" pm's

      H_2 (.3 m x .6 m) use 18 - 2" pm's

   b) Shower-Veto - These are made with two layers of lead and two layers of scintillators.

      Sh 1 .5 m x 2 m use 4 - 2" pm's

      Sh 2 2.5 m x 3 m use 30 - 2" pm's

      Sh 3 2 m x 4 m use 16 - 2" pm's

   c) Solid state hodoscope (H3)

      This is made by two totally depleted surface barrier solid state counters, each with its collector plate in the form of an array of individual strips 0.2 mm wide. The area of this hodoscope is 2 cm x 2 cm.

   d) Gas Cerenkov counter - This counter has been described in Section II-D. It consists of a 10 meter long light tight box, a 3 m x 1.5 m mirror and around eight 2" photomultipliers.

2. Wire Spark Chamber

All are standard magnetostrictive readout wire chambers except for those inside the target magnet. These, due to the strong magnetic field, will use capacitive readout or will have the chamber wires extended outside the strong field region so magnetostrictive readout can be used. The number of chambers and their sizes are listed below.

Size	No.
.5 m x .5 m	3
.5 m x 1.25 m	2
.3 m x .5 m	1
1 m x 2 m	7
2 m x 2 m	10

3. Fast Electronics

The Caltech group owns a large assortment of fast electronic models that will be more than sufficient to operate this experiment.

4. Computer and Interface

A Sigma 2 computer with a complete set of peripherals and interface as described in Section III-C will be provided by the Caltech group.

The main items to be furnished by NAL are:

1. Target - A 30 cm. long, $\frac{1}{2}$ cm. diameter cell with .010" mylar entrance and exit windows.

2. Target Magnet - This C magnet should have a gap size at 0.6 m x 0.6 m x 2 m with 18 Kg at the pole tip. This magnet is described in Section II-B-2. We feel that this magnet can be constructed relatively inexpensively by using flame cut armor plate in the return yoke.
3. Forward Spectrometer Magnet - This is a standard H magnet with a gap of 0.5 m x 1 m x 2 m with a field of 18 Kg.
4. Power supplies to run the above magnets.
5. Beam Requirements - Unseparated beam of both polarities with the following characteristics:

Intensity	$\geq 10^6$ π/pulse
Diameter	1 mm
Divergence	$\leq$ .3 mr
$\frac{\Delta p}{p}$	$\pm$ 0.5%

The small divergence and size required can easily be relaxed by adding small beam hodoscopes.